coupling and possibly to delocalization. The concentration and identity of cations and anions control the extent of coupling, as shown by far-IR, ^{23}Na MAS NMR, and UV-visible spectroscopy. Results from optical spectroscopy and extended Hückel molecular orbital calculations hinted at the evolution of narrow bands. Very recent studies of the Ag^+ loading dependent ^{23}Na quadrupole coupling constants (DOR NMR) and ^{81}Br,^{35}Cl chemical shifts (MAS NMR) in class A and class B sodium,silver halosodalites provide convincing evidence for collective electronic interactions between $Na_{4-n}Ag_nX$ clusters in the sodalite lattice.[28a,b]

Acknowledgment. We acknowledge the Natural Science and Engineering Research Council (NSERC) of Canada's Operating and Strategic Grants Programmes, Alcan Canada and Optical Recording Corporation, Toronto (G.A.O.), as well as the Office of Naval Research and QUEST (G.D.S.) for generous financial support of this work. A.S. thanks NSERC for a 1967 Science and Engineering Postgraduate Scholarship. We thank Raz Jelinek, Peter M. Macdonald, Michele Meszaros, Bill Harrison, and Nancy Keder for valuable technical assistance and discussions.

Supplementary Material Available: Tables of crystallographic characterization data for NaBr-SOD, $Na_{7.6}Ag_{0.3}Br$-SOD, $Na_{5.3}Ag_{2.4}Br$-SOD, AgBr-SOD, AgCl-SOD, and AgI-SOD (6 pages). Ordering information is given on any current masthead page.

Structure and Properties of Molybdenum(IV,V) Arenethiolates with a Neighboring Amide Group. Significant Contribution of NH···S Hydrogen Bond to the Positive Shift of Redox Potential of Mo(V)/Mo(IV)

Norikazu Ueyama, Taka-aki Okamura, and Akira Nakamura*

Contribution from the Department of Macromolecular Science, Faculty of Science, Osaka University, Toyonaka, Osaka 560, Japan. *Received February 24, 1992*

Abstract: Monooxomolybdenum(V) and monooxomolybdenum(IV) complexes with *o*-(acylamino)benzenethiolate, $(NEt_4)[Mo^VO(S\text{-}o\text{-}RCONHC_6H_4)_4]$ (R = CH_3, *t*-Bu, CF_3), $(NEt_4)_2[Mo^{IV}O(S\text{-}o\text{-}RCONHC_6H_4)_4]$, were synthesized and characterized by visible, ESR, ^1H NMR, and Raman spectroscopies, and electrochemical analysis. $(PPh_4)[Mo^VO(S\text{-}o\text{-}CH_3CONHC_6H_4)_4]\cdot CH_3CN$ crystallizes in the space group $P2_1/n$ with a = 20.95 (2) Å, b = 12.509 (2) Å, c = 22.383 (5) Å, β = 91.8 (1)°, V = 5864 (8) Å^3, Z = 4, and d_{calcd} = 1.311 g cm^{-3}. $(PPh_4)_2[Mo^{IV}O(S\text{-}o\text{-}CH_3CONHC_6H_4)_4]$ crystallizes in the space group $P2_1$ with a = 14.636 (3) Å, b = 13.457 (3) Å, c = 19.341 (2) Å, β = 110.08 (1)°, V = 3578 (1) Å^3, Z = 2, and d_{calcd} = 1.351 g cm^{-3}. Both complexes have a distorted square-pyramidal structure with an axial Mo=O and two distinct kinds of Mo-S bonds. All four acylamino groups of both complexes are located at the Mo=O side even in spite of the steric neighboring congestion which is similar to the reported structure of $(NEt_4)[Mo^VO(SC_6H_5)_4]$. All four NH groups are involved in intraligand NH···S hydrogen bonds with which contribute to the positive shift of Mo(V)/Mo(IV) redox potential in acetonitrile. Preliminary EHMO calculations also support the NH···S hydrogen bonds.

Introduction

Monooxomolybdenum(V) and monooxomolybdenum(IV) complexes having thiolate ligands are of interest as model complexes for resting or reduced species of the active site of biologically important molybdooxidases. The very rapid and rapid signals appeared on the reduction of the enzymes have been considered to be dioxomolybdenum(V) species. However, a synthetic model complex $[Mo^VO_2L]^-$ (LH_2 = *N*,*N*'-dimethyl-*N*,*N*'-bis(2-mercaptophenyl)-1,2-diaminoethane), has been considered to convert to the monooxomolybdenum(V) species in the presence of protons.[1] Crystallographic and spectroscopic analyses of various monooxomolybdenum(V) complexes containing ligand sets, e.g., S_4, S_2N_2, S_2O_2, and N_3S_2, have been reported.[2-15] For example, arenethiolate complexes, $[Mo^VO(SPh)_4]^{-3}$ and $[Mo^VO(bdt)_2]^-$ (bdt = 1,2-benzenedithiolato),[16] and alkanedithiolate complexes, $[Mo^VO(SCH_2CH_2S)_2]^-$,[9] are known to have a square-pyramidal geometry. The ESR parameters in $[MoOCl_{4-x}(SPh)_x]^-$ (x = 0-4) have been shown to be related to the number of thiolate ligands and the covalency of the Mo-S bonds.[17] Nonpyramidal mono-

(1) Wilson, G. L.; Greenwood, R. J.; Pilbrow, J. R.; Spence, J. T.; Wedd, A. G. *J. Am. Chem. Soc.* **1991**, *113*, 6803.
(2) Yamanouchi, K.; Enemark, J. H. *Inorg. Chem.* **1979**, *18*, 1626.
(3) Boyd, I. W.; Dance, I. G.; Murray, K. S.; Wedd, A. G. *Aust. J. Chem.* **1978**, *31*, 279.
(4) Bradbury, J. R.; Mackay, M. F.; Wedd, A. G. *Aust. J. Chem.* **1978**, *31*, 2423.
(5) Taylor, R. D.; Street, J. P.; Minell, M.; Spence, J. T. *Inorg. Chem.* **1978**, *17*, 3207.
(6) Scullane, M. I.; Taylor, R. D.; Minelli, M.; Spence, J. T.; Yamanouchi, K.; Enemark, J. H.; Chasteen, N. D. *Inorg. Chem.* **1979**, *18*, 3213.
(7) Bishop, P. T.; Dilworth, J. R.; Hutchinson, J.; Zubieta, J. A. *J. Chem. Soc., Chem. Commun.* **1982**, 1052.
(8) Kaul, B. B.; Enemark, J. H.; Merbs, S. L.; Spence, J. T. *J. Am. Chem. Soc.* **1985**, *107*, 2885.
(9) Ellis, S. R.; Collison, D.; Garner, C. D.; Clegg, W. *J. Chem. Soc., Chem. Commun.* **1986**, 1483.
(10) Dowerah, D.; Spence, J. T.; Singh, R.; Weed, A. G.; Wilson, G. L.; Farchione, F.; Enemark, J. H.; Kristofzski, J.; Bruck, M. *J. Am. Chem. Soc.* **1987**, *109*, 5655.
(11) Ueyama, N.; Yoshinaga, N.; Kajiwara, A.; Nakamura, A.; Kusunoki, M. *Bull. Chem. Soc. Jpn.* **1991**, *64*, 2458.
(12) Chang, C. S. J.; Collison, D.; Mabbs, F. E.; Enemark, J. H. *Inorg. Chem.* **1990**, *29*, 2261.
(13) Sanz, V.; Picher, T.; Palanca, P.; Gomez-Romero, P.; Llopis, E.; Ramírez, J. A.; Beltran, D.; Cervilla, A. *Inorg. Chem.* **1991**, *30*, 3113.
(14) Cleland, W. E. J.; Barnhart, K. M.; Yamanouchi, K.; Collison, D.; Mabbs, F. E.; Ortega, R. B.; Enemark, J. H. *Inorg. Chem.* **1987**, *26*, 1017.
(15) Pickett, C.; Kumar, S.; Vella, P. A.; Zubieta, J. *Inorg. Chem.* **1982**, *21*, 908.
(16) Boyde, S.; Ellis, S. R.; Garner, C. D.; Clegg, W. *J. Chem. Soc., Chem. Commun.* **1986**, 1541.

0002-7863/92/1514-8129$03.00/0

oxomolybdenum(V) and molybdenum(IV) complexes with a ligand set N_3S or N_3S_2 have also been systematically studied using a tridentate chelating ligand, e.g., hydrotris(3,5-dimethyl-1-pyrazolyl)borate ($HB(3,5\text{-}Me_2pz)_3$).[14,18-21]

Only a few monooxomolybdenum(IV) complexes with four thiolate ligands have been characterized because of difficulty in the isolation, e.g., $[Mo^{IV}O(bdt)_2]^{2-}$,[16] $[Mo^{IV}O(SC_6F_5)_4]^{2-}$,[22] $[Mo^{IV}O\{S_2C_2(CO_2Me)\}_2]^{2-}$,[23] and $[Mo^{IV}O(SCH_2CH_2S)_2]^{2-}$.[24] Various oxomolybdenum(IV) complexes containing ligand sets other than S_4 have been also characterized.[8,25-28]

A unique chelating peptide fragment, Cys-X-Y-Cys (X, Y = amino acid residues), has been found in the active site of various kinds of metalloproteins, e.g., rubredoxin,[29] alcohol dehydrogenase,[30] and aspartate carbamoyltransferase.[31] In a previous paper, we reported that a chelating peptide complex, $[Mo^{V}O(Z\text{-cys-Pro-Leu-cys-OMe})_2]^-$ (Z = benzyloxycarbonyl), has two isomers consisting of parallel and antiparallel orientations of two peptide chains. The parallel isomer exhibits a remarkably positive-shifted redox potential of the couple, Mo(V)/Mo(IV), in acetonitrile and can be readily reduced to the Mo(IV) state by a mild reductant.[32] The origin of the positive shift has been considered to come from the interaction between the amide NH group and thiolate sulfur atom or from the perturbation to Mo=O group by amide NH. To examine the effect of NH···S bonding in oxomolybdenum complexes, we have prepared a variation of the benzenethiolate ligand with an *o*-acylamino substituent.

The presence of NH···S hydrogen bonds has been shown to be one of the important factors for the positive shifts of the redox potentials of reduced rubredoxin model complexes, especially in nonpolar solvent, e.g., $[Fe^{II}(Z\text{-cys-Pro-Leu-cys-OMe})_2]^{2-}$, $[Fe^{II}(Z\text{-cys-Pro-Leu-cys-Gly-NH-}p\text{-substituted } C_6H_4)_2]^{2-}$,[33] and ferredoxin peptide-model complexes.[34-36] The presence of interionic NH···S hydrogen bonds has also been reported for $[(CH_3)_3NCH_2CONH_2]_2[Co(SC_6H_5)_4]\cdot{}^1/_2CH_3CN$[37] in the solid state and in the intramolecular version for $[\mu\text{-}N_2H_4\{Fe(bdt)_2\}_2]^{2-}$.[38]

A nearby NH proton or the other proton source of molybdenum active center is also important in the coupled proton and electron-transfer process.[39,40]

Experimental Section

All procedures were performed in argon atmosphere by the Schlenk technique. All solvents were dried and distilled under argon before use.

Tetraethylammonium monooxotetrakis(benzenethiolalo)molybdenum(V) and the ortho- or para-methoxy-substituted complexes were prepared by the reported method.[3] Bis[*o*-(acetylamino)phenyl] disulfide, bis[*o*-(pivaloylamino)phenyl] disulfide, bis[*o*-{(trifluoroacetyl)amino}phenyl] disulfide,[41] and 2,2′-dithiobis(*N*-methylaniline) were prepared by the literature procedures.[42,43]

Preparation of 2,2′-Dithiobis(*N*-phenylacetamide). To a pyridine solution (60 mL) of 2,2′-dithiodianiline (15 g, 60 mmol) was added acetyl chloride (9.5 g, 120 mmol) at 0 °C and dichloromethane (100 mL) at room temperature to give a clear solution. After stirring overnight, the solution was concentrated under reduced pressure. The residue was dissolved in chloroform, and the chloroform layer was washed with 2% aqueous HCl solution, water, 4% aqueous $NaHCO_3$ solution, and water successively. The organic layer was dried over magnesium sulfate and concentrated under reduced pressure to give white solid which was recrystallized from chloroform/methanol/diethyl ether: yield 17 g (86%); ^1H NMR (chloroform-d_1) δ 1.97 (s, 6 H), 7.02 (t, 2 H), 7.42 (m, 4 H), 7.90 (s, 2 H), 8.34 (d, 2 H). Anal. Calcd for $C_{16}H_{16}N_2O_2S_2$: C, 57.81; H, 4.85; N, 8.43; S, 19.29. Found: C, 57.55; H, 4.92; N, 8.35; S, 19.10.

Preparation of 2,2′-Dithiobis(*N*-phenyl-2,2-dimethylpropanamide). The compound was synthesized by the same method as described for 2,2′-dithiobis(*N*-phenylacetamide). The crude material was recrystallized from hot *n*-hexane: yield 89%; ^1H NMR (chloroform-d_1) δ 1.24 (s, 18 H), 6.94 (t, 2 H), 7.21 (d, 2 H), 7.36 (t, 2 H), 8.46 (d, 2 H), 8.52 (s, 2 H). Anal. Calcd for $C_{22}H_{28}N_2O_2S_2$: C, 63.43; H, 6.77; N, 6.72; S, 15.39. Found: C, 63.37; H, 6.67; N, 6.72; S, 15.34.

Preparation of 4,4′-Dithiobis(*N*-phenyl-2,2-dimethylpropanamide). The compound was synthesized by the same method as described for 2,2′-dithiobis(*N*-phenylacetamide). The crude material was recrystallized from tetrahydrofuran (THF)/diethyl ether: yield 99%; ^1H NMR (Me_2SO-d_6) δ 1.22 (s, 18 H), 7.2 (d, 4 H), 7.3 (d, 4 H), 9.1 (s, 2 H). Anal. Calcd for $C_{22}H_{28}N_2O_2S_2(H_2O)_{0.5}(C_4H_8O)$: C, 62.74; H, 7.49; N, 5.63; S, 12.89. Found: C, 62.51; H, 7.21; N, 5.69; S, 13.08.

Preparation of 2,2′-Dithiobis(*N*-phenyl-2,2,2-trifluoroacetamide). The compound was prepared from 2,2′-dithiodianiline and trifluoroacetic acid anhydride. The crude material was recrystallized from ethyl acetate/*n*-hexane: yield 91%; ^1H NMR (chloroform-d_1) δ 7.18 (t, 2 H), 7.37 (d, 2 H), 7.50 (t, 2 H), 8.35 (d, 2 H), 8.78 (s, 2 H). Anal. Calcd for $C_{16}H_{10}N_2O_2F_6S_2$: C, 43.64; H, 2.29; N, 6.36. Found: C, 43.42; H, 2.35; N, 6.35.

Preparation of 2,2′-Dithiobis(*N*-methyl-*N*-phenylacetamide). The compound was synthesized from 2,2′-dithiobis(*N*-methylaniline) and acetyl acetyl chloride by the same method as described for 2,2′-dithiobis(*N*-phenyl acetamide). The crude material was recrystallized from ethyl acetate/*n*-hexane: yield 57%; ^1H NMR (chloroform-d_1) δ 1.85 (s, 6 H), 3.24 (s, 6 H), 7.22 (d, 2 H), 7.30 (t, 2 H), 7.39 (t, 2 H), 7.68 (d, 2 H). Anal. Calcd for $C_{18}H_{20}N_2O_2S_2$: C, 59.97; H, 5.59; N, 7.77. Found: C, 59.36; H, 5.70; N, 7.52.

Synthesis of $(NEt_4)[Mo^{V}O(S\text{-}o\text{-}CH_3CONHC_6H_4)_4]$ (1a). The complex was synthesized by the ligand exchange method. A mixture of $(NEt_4)[Mo^{V}O(SPh)_4]$ (140 mg, 0.2 mmol) and 2,2′-dithiobis(*N*-phenylacetamide) (500 mg, 1.5 mmol) in THF (8 mL) was stirred at room temperature overnight. The precipitate was collected by filtration and washed with 1,2-dimethoxyethane (DME). The deep purple crude product was recrystallized from acetonitrile/diethyl ether, and deep purple microcrystals were obtained: yield 130 mg (71%). Anal. Calcd for $C_{40}H_{52}N_5O_5S_4Mo$: C, 52.97; H, 5.78; N, 7.72. Found: C, 52.77; H, 5.86; N, 7.72.

Synthesis of $(PPh_4)[Mo^{V}O(S\text{-}o\text{-}CH_3CONHC_6H_4)_4]\cdot CH_3CN$ (1a′). The complex was synthesized by the same method described for the synthesis of **1a** using the PPh_4^+ salt. Deep purple crystals were obtained from hot acetonitrile/diethyl ether in 43% yield. Anal. Calcd for $C_{58}H_{55}N_5O_5PS_4Mo$: C, 60.20; H, 4.79; N, 6.05. Found: C, 60.22; H, 5.02; N, 5.93.

(17) Hanson, G. R.; Brunette, A. A.; Mcnell, A. C.; Murray, K. S.; Wedd, A. G. *J. Am. Chem. Soc.* **1981**, *103*, 1953.
(18) Young, C. G.; Enemark, J. H.; Collison, D.; Mabbs, F. E. *Inorg. Chem.* **1987**, *26*, 2926.
(19) Young, C. G.; Enemark, J. H. *Inorg. Chem.* **1985**, *24*, 4416.
(20) Roberts, S. A.; Young, C. G.; W. E.; Cleland, J.; Ortega, R. B.; Enemark, J. H. *Inorg. Chem.* **1988**, *27*, 3044.
(21) Young, C. G.; Roberts, S. A.; Ortega, R. B.; Enemark, J. H. *J. Am. Chem. Soc.* **1987**, *109*, 2938.
(22) Ellis, S. R.; Collison, D.; Garner, C. D. *J. Chem. Soc., Dalton Trans.* **1989**, 413.
(23) Coucouvanis, D.; Hadjikyriacou, A.; Toupadakis, A.; Koo, S.; Ileperuma, O.; Draganjac, I. M.; Salifoglou, A. *Inorg. Chem.* **1991**, *30*, 754.
(24) Mitchell, P. C. H.; Pygall, C. F. *Inorg. Chim. Acta* **1979**, *33*, L109.
(25) Rice, C. A.; Spence, J. T. *Inorg. Chem.* **1980**, *19*, 2845.
(26) Bishop, P. T.; Dilworth, J. R.; Hughes, D. L. *J. Chem. Soc., Dalton Trans.* **1988**, 2535.
(27) Burrow, T. E.; Hills, A.; Hughes, D. L.; Lane, J. D.; Morris, R. H. *J. Chem. Soc., Dalton Trans.* **1990**, 1813.
(28) Schneider, P. W.; Bravard, D. C.; McDonald, J. W.; Newton, W. E. *J. Am. Chem. Soc.* **1972**, 8640.
(29) Orme-Johnson, W. H. *Annu. Rev. Biochem.* **1973**, *42*, 109.
(30) Eklund, H.; Nordström, B.; Zeppezauer, E.; Söderlund, G.; Ohlsson, I.; Boiwe, T. L.; Sonderberg, B. O.; Tapia, O.; Bränden, C. I. *J. Mol. Biol.* **1976**, *102*, 27.
(31) Monaco, H. L.; Crawford, J. L.; Lipscomb, W. N. *Proc. Natl. Acad. Sci. U.S.A.* **1978**, *75*, 5276.
(32) Ueyama, N.; Yoshinaga, N.; Kajiwara, A.; Nakamura, A. *Chem. Lett.* **1990**, 1781.
(33) Sun, W.; Ueyama, N.; Nakamura, A. *Inorg. Chem.* **1991**, *30*, 4026.
(34) Ueyama, N.; Terakawa, T.; Nakata, M.; Nakamura, A. *J. Am. Chem. Soc.* **1983**, *105*, 7098.
(35) Ueyama, N.; Nakata, M.; Fuji, M.; Terakawa, T.; Nakamura, A. *Inorg. Chem.* **1985**, *24*, 2190.
(36) Ohno, R.; Ueyama, N.; Nakamura, A. *Inorg. Chem.* **1991**, *30*, 4887.
(37) Walters, M. A.; Dewan, J. C.; Min, C.; Pinto, S. *Inorg. Chem.* **1991**, *30*, 2656.
(38) Sellmann, D.; Soglowek, W.; Knoch, F.; Moll, M. *Angew. Chem., Int. Ed. Engl.* **1989**, *28*, 1271.
(39) George, G. N.; Bray, R. *Biochemistry* **1988**, *27*, 3603.
(40) Stiefel, E. I. *Proc. Natl. Acad. Sci. U.S.A.* **1973**, *70*, 988.
(41) Young, R. N.; Gauthier, J. Y.; Coombs, W. *Tetrahedron Lett.* **1984**, *25*, 1753.
(42) Kiprianov, A. I.; Pazenko, Z. N. *Zh. Obshch. Khim.* **1949**, *19*, 1523.
(43) Ohtsuka, Y.; Oishi, T. *Chem. Pharm. Bull.* **1983**, *31*, 454.

Synthesis of $(NEt_4)[Mo^VO(S\text{-}o\text{-}t\text{-}BuCONHC_6H_4)_4]$ (2a). The complex was synthesized by a method similar to that described for $(NEt_4)[Mo^VO(S\text{-}o\text{-}CH_3CONHC_6H_4)_4]$. A mixture of $(NEt_4)[Mo^VO(SPh)_4]$ (80 mg, 0.12 mmol) and 2,2′-dithiobis(*N*-phenyl-2,2-dimethylpropanamide) (120 mg, 0.28 mmol) in DME (3 mL) was stirred at room temperature overnight. The red-purple precipitate was collected by filtration and washed with diethyl ether. The crude product was recrystallized from acetonitrile/diethyl ether, and red-purple microcrystals were obtained: yield 93 mg (73%). Anal. Calcd for $C_{52}H_{76}N_5O_5S_4Mo$: C, 58.08; H, 7.12; N, 6.15. Found: C, 57.98; H, 7.21; N, 6.55.

Synthesis of $(NEt_4)[Mo^VO(S\text{-}p\text{-}t\text{-}BuCONHC_6H_4)_4]$. *N*-(4-Mercaptophenyl)-2,2-dimethylpropanamide was prepared by the reduction of 4,4′-dithiobis(*N*-phenyl-2,2-dimethylpropanamide) with sodium borohydride in ethanol/THF. The complex was synthesized by a method similar to that described for **2a**, except that the thiol instead of the disulfide was used. The blue precipitate was collected by filtration and washed with DME and diethyl ether. The crude product was recrystallized from hot acetonitrile/diethyl ether: yield 65 mg (49%). Anal. Calcd for $C_{52}H_{76}N_5O_5S_4Mo$: C, 58.08; H, 7.12; N, 6.51. Found: C, 57.05; H, 7.37; N, 6.81.

Synthesis of $(NEt_4)[Mo^VO(S\text{-}o\text{-}CF_3CONHC_6H_4)_4]$. The compound was synthesized by the same method described for **1a**: yield 58%. Anal. Calcd for $C_{40}H_{40}N_5O_5F_{12}S_4Mo$: C, 42.78; H, 3.59; N, 6.24. Found: C, 42.68; H, 3.82; N, 6.14.

Synthesis of $(NEt_4)[Mo^VO\{S\text{-}o\text{-}CH_3CON(CH_3)C_6H_4\}_4]$. The compound was prepared by the method described for **1a**, except the ligand exchange reaction required a continuous stirring for 2 days: yield 37%. Anal. Calcd for $C_{44}H_{60}N_5O_5S_4Mo$: C, 54.87; H, 6.28; N, 7.27. Found: C, 54.21; H, 6.30; N, 7.16.

Synthesis of $(NEt_4)_2[Mo^{IV}O(S\text{-}o\text{-}CH_3CONHC_6H_4)_4]$ (1b). To a THF solution (50 mL) of $(NEt_4)[Mo^VO(S\text{-}o\text{-}CH_3CONHC_6H_4)_4]$ (**1a**) (320 mg, 0.35 mmol) was added tetraethylammonium borohydride (65 mg, 0.48 mmol) at 0 °C. The solution was stirred for 4 h at room temperature. The precipitate was collected by filtration and washed with THF until washing solutions were colorless. The crude powder was dissolved in 15 mL of acetonitrile and filtered to remove insoluble materials. The solution was concentrated under reduced pressure, and the residue was recrystallized from acetonitrile/diethyl ether to give extremely air-sensitive, light-blue crystals in 38% yield. Anal. Calcd for $C_{48}H_{72}N_6O_5S_4Mo$: C, 55.58; H, 7.00; N, 8.10. Found: C, 54.75; H, 7.44; N, 7.84.

Synthesis of $(Ph_4P)_2[Mo^{IV}O(S\text{-}o\text{-}CH_3CONHC_6H_4)_4]$ (1b′). The reduction of **1a** was carried out by the same procedure as described for **1b**. To a solution reduced by tetraethylammonium borohydride was added an acetonitrile solution of tetraphenylphosphonium bromide (2.4 molar), and the solution was allowed to stand at room temperature. Green-blue needles precipitated and were collected by filtration and washed with acetonitrile. The crystals were recrystallized from acetonitrile/diethyl ether in 55% yield. Anal. Calcd for $C_{80}H_{72}N_4O_5P_2S_4Mo$: C, 66.01; H, 4.99; N, 3.85. Found: C, 65.87; H, 5.06; N, 3.84.

Synthesis of $(NEt_4)_2[Mo^{IV}O(S\text{-}o\text{-}t\text{-}BuCONHC_6H_4)_4]$. The complex was synthesized by the same method described for **1b**. Purple-red plates were obtained in 40% yield. Anal. Calcd for $C_{60}H_{96}N_6O_5S_4Mo$: C, 59.77; H, 8.03; N, 6.97. Found: C, 59.47; H, 8.18; N, 6.93.

Synthesis of $(NEt_4)_2[Mo^{IV}O(S\text{-}o\text{-}CF_3CONHC_6H_4)_4]$. The complex was synthesized by the same method described for **1b**. Red-brown plates were obtained in 74% yield. Anal. Calcd for $C_{48}H_{60}N_6O_5F_{12}S_4Mo$: C, 46.00; H, 4.83; N, 6.71. Found: C, 46.08; H, 5.00; N, 6.73.

Physical Measurements. Visible spectra were recorded in solution on a Jasco Ubest-30 spectrophotometer. ^1H NMR spectra were taken on Jeol GSX-400 spectrometer in acetonitrile-d_3 solution. Raman spectrum was obtained on a Jasco R-800 spectrophotometer equipped with a HTV-R649 photomultiplier. A solid sample in a capillary was irradiated with a 514.5-nm Ar^+ laser excitation line. The frequency calibration of the spectrometer was carried out with indene as a standard. IR spectra were recorded on a Jasco DS-402G spectrometer. Samples were prepared as KBr pellets. Electrochemical measurements were carried out using a Yanaco P-1100 instrument in acetonitrile solution that contained 0.1 M tetra-*n*-butylammonium perchlorate as a supporting electrolyte. $E_{1/2}$ value, determined as $(E_{p,a} + E_{p,c})/2$, was referenced to the SCE electrode at room temperature, and a value uncorrected for junction potential was obtained. In the same condition, ferrocene/ferrocenium redox couple was observed at +0.39 V vs SCE. ESR spectra in *N*,*N*-dimethylformamide (DMF)/acetonitrile (1/4 v/v) were recorded on a Jeol JES-FE1X spectrometer at room temperature and at ca. 80 K.

X-ray Structure and Determination. Single crystals of $(PPh_4)[Mo^VO(S\text{-}o\text{-}CH_3CONHC_6H_4)_4]\cdot CH_3CN$ (**1a′**) and $(PPh_4)_2[Mo^{IV}O(S\text{-}o\text{-}CH_3CONHC_6H_4)_4]$ (**1b′**) were sealed in a glass capillary under argon atmosphere for the X-ray measurements. X-ray measurements were performed at 23 °C on a Rigaku AFC5R diffractometer equipped with a rotating anode X-ray generator. The radiation used was Mo Kα monochromatized with graphite (0.71069 Å). No absorption correction was made for **1a′**. An empirical absorption correction based on azimuthal scans of several reflections was applied for **1b′**, and transmission factors ranged from 0.96 to 1.00. The basic crystallographic parameters for **1a′** and **1b′** are listed in Table I. Unit cell dimensions were refined with 25 reflections. Three standard reflections were chosen and monitored with every 100 reflections and did not show any significant change. At a lower angle θ ($3° < 2\theta < 40°$) sufficient reflections, 86% (**1a′**) and 71% (**1b′**), were observed. However, at a higher angle the intensities of reflections were weakened by the thermal motion of the amide groups and acetonitrile in the crystal. The structures were solved by the direct method using TEXSAN crystallographic software package of the Molecular Structure Corp. The non-hydrogen atoms were refined anisotropically. Hydrogen atoms were placed on the calculated positions. The final refinement was carried out using full-matrix least-squares techniques with non-hydrogen atoms. The *y* coordinate of the molybdenum atom for **1b′** was fixed in the refinement. Since space group $P2_1$ is an acentric space group, both enantiomers for **1b′** were refined to determine the correct enantiomer. The incorrect enantiomer shows a little larger *R* factor (0.049), a shorter Mo=O distance (1.676 (5) Å), and a wider range of Mo–S distances (2.425 (2) – 2.398 (2) Å). The final difference Fourier map showed no significant features. Atom scattering factors and dispersion corrections were taken from the *International Tables for X-ray Crystallography*.[44]

EHMO Calculations. The extended Hückel MO calculations of $[Mo^VO(cis\text{-}SCH{=}CHNHCHO)_4]^-$ as a simple model of $[Mo^VO(S\text{-}o\text{-}CH_3CONHC_6H_4)_4]^-$ using a NEC PC-98 EHMO program obtained from Kodansha Sci. Co. was performed. Dependence of Mo=O, Mo–S, NH···S, NH···O, and S–C overlap populations on rotation of S–C torsion angle was examined in the above complex to evaluate the distortion of the Mo^VOS_4 core and the NH···S hydrogen bonding.

Mo–O, Mo–S, S–C, C=C, and C–H bond distances used are 1.680, 2.397, 1.773, 1.400, and 1.090 Å, respectively. A value, −68.8°, was employed for O–Mo–S–C torsion angles. All atoms of SCH=CHNHCHO group were placed in one plane. The mean bond angles, 108.8° and 110.2°, were adopted for O–Mo–S and Mo–S–C, respectively. The EHMO atomic parameters for Mo(V) were taken from the literature.[45]

Results

Synthesis. Monooxomolybdenum(V) *o*-(acylamino)benzenethiolate (SAr) complexes were synthesized by the ligand exchange reaction as shown below. The synthesis of $(NEt_4)[Mo^VO(SPh)_4]$

$$(NEt_4)[Mo^VO(SPh)_4] + ArSSAr \xrightarrow[\text{in DME or THF}]{} (NEt_4)[Mo^VO(SAr)_4] + PhSSPh$$

has been reported by Wedd et al.[3] A similar ligand exchange reaction with a redox process has been employed for the synthesis of $[Fe_4S_4(SePh)_4]^{2-}$ from $[Fe_4S_4(S\text{-}t\text{-}Bu)_4]^{2-}$ and $(SePh)_2$.[46] Arenethiolate complexes of molybdenum(V), $(NEt_4)[Mo^VO(SAr)_4]$, can be successfully isolated due to the low solubility of the complex in DME.

Synthesis of monooxomolybdenum(IV) thiolate complexes has been difficult because of the poor yield when $[Mo^{IV}O_2(CN)_4]^{4-}$ was used as a starting material, e.g., $(NEt_4)_2[Mo^{IV}O(ethanedithiolato)_2]$, $(NEt_4)_2[Mo^{IV}O(bdt)_2]$.[16,24] On the other hand, ortho-substituted benzenethiolate Mo(IV) complex can be easily synthesized in the presence of a weak reductant, e.g., NEt_4BH_4, under mild conditions as in the following.

$$(NEt_4)[Mo^VO(SAr)_4] \xrightarrow{NEt_4BH_4} (NEt_4)_2[Mo^{IV}O(SAr)_4]$$

Crystal Structure of $(PPh_4)[Mo^VO\{o\text{-}(acetylamino)benzenethiolato\}_4]\cdot CH_3CN$ (1a′) and $(PPh_4)_2[Mo^{IV}O\{o\text{-}(acetylamino)benzenethiolato\}_4]$ (1b′). The monooxomolybdenum(V) complex, **1a′**, crystallizes in a space group $P2_1/n$ and contains four anions and four $(PPh_4)^+$ cations. The ORTEP view of the anions is shown in Figure 1. All four *o*-acetylamino groups are favorably located in the same side of Mo=O group in spite of the steric congestion. The arene (Ar) plane is perpendicular to the Mo–S–C plane. The

(44) Cromer, D. T. *International Tables for X-ray Crystallography*; The Kynoch, Press: Birmingham, England, 1974; Vol. IV, Table 2.2A.
(45) Kamata, M.; Hirotsu, K.; Higuchi, K.; Tatsumi, K.; Hoffmann, R.; Yoshida, T.; Otsuka, S. *J. Am. Chem. Soc.* **1981**, *103*, 5772.
(46) Que, L., Jr.; Bobrik, M. A.; Ibers, J. A.; Holm, R. H. *J. Am. Chem. Soc.* **1974**, *96*, 4168.

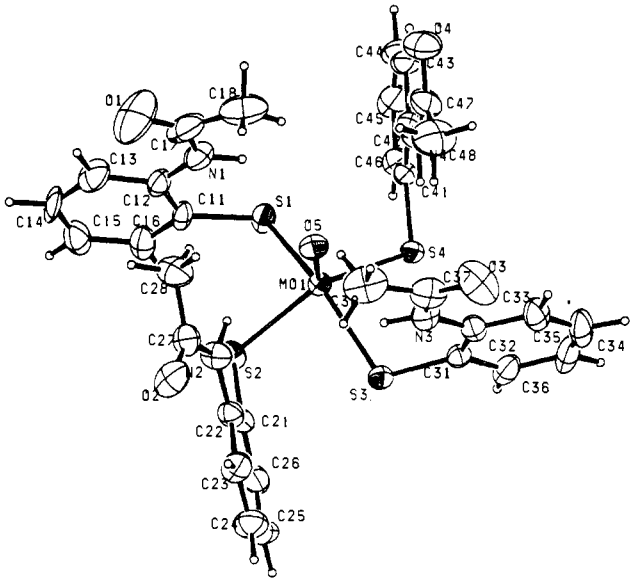

Figure 1. Perspective view of the anion part of $(PPh_4)[Mo^{V}O(S\text{-}o\text{-}CH_3CONHC_6H_4)_4]\cdot CH_3CN$.

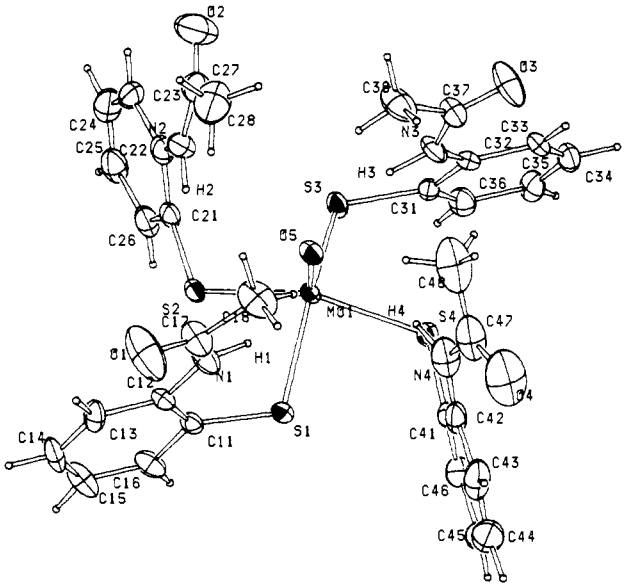

Figure 2. Perspective view of the anion part of $(PPh_4)_2[Mo^{IV}O(S\text{-}o\text{-}CH_3CONHC_6H_4)_4]$.

Ar orientation (mean 72.8°) against the Mo–S–C plane is larger than the favorable location (mean 44.5°) of the phenyl group in $(AsPh_4)[Mo^{V}O(SPh)_4]$.[4]

Figure 2 shows the ORTEP view of the anion part of Mo(IV) complex (**1b′**) which has two molecules per unit cell in space group $P2_1$. All four Ar groups are similarly located in the same side of Mo=O and are roughly perpendicular (mean 69.8°) to the Mo–S–C plane as the crystal structure of **1a′**.

Selected bond distances and bond angles for the both complexes are listed in Table II. The Mo=O distance (1.679 (4) Å in **1a′** is not significantly different from that (1.689 (5) Å) in **1b′** and is close to that (1.669 (9) Å) of $[Mo^{V}O(SPh)_4]^-$.[4] Clegg et al. have demonstrated the elongation (1.699 (6) Å) of Mo=O distance in $[Mo^{IV}O(bdt)_2]^{2-}$ when compared with that (1.668 (3) Å) of $[Mo^{V}O(bdt)_2]^-$,[16] because the reduction of the Mo(V) site leads to a more electron-rich Mo(IV) site. Two kinds of Mo–S distances are observed in **1a′**. The longer Mo–S(1) and Mo–S(3) distances (mean 2.405 Å) are close to those of (mean 2.403 Å) $[Mo^{V}O(SPh)_4]^-$.[4] The shorter Mo–S(2) and Mo–S(4) distances (mean 2.387 Å) are similar to those (mean 2.382 Å) of $[Mo^{V}O(HB(3,5\text{-}Me_2pz)_3)(SPh)_2]$.[14] The difference in mean Mo–S distance between **1a′** and **1b′** is approximately 0.01 Å similar to the difference (0.01 Å) for $[Mo^{V}O(bdt)_2]^-$ and $[Mo^{IV}O(bdt)_2]^{2-}$.

On the other hand, a notable angular difference (12.8°) between S(1)–Mo–S(3) (148.9 (1)°) and S(2)–Mo–S(4) (136.1 (1)°) was found, whereas only a small difference (3.5°) in $[Mo^{V}O(SPh)_4]^-$ was reported. A distortion from square-pyramidal geometry in Mo(V) was found for $[Mo^{V}O(1,3\text{-propanedithiolato})_2]^-$ with a significant difference (9.1°)[7] and for $[Mo^{V}O(\alpha,2\text{-toluenedithiolato})_2]^-$ with a larger difference (14°)[11] which is of course due to the asymmetrical chelating dithiolate ligand.

Table II also lists the N(H)–S bond distances (2.97–3.03 Å) which indicates the close location of the amide NH to the adjacent arenethiolate sulfur atom. The coplanarity of the amide group and the benzene ring favors π-conjugation and hydrogen bonding of the NH group to the sulfur atom rather than O atom on Mo. Although the sterically preferable location of the amide is at the position where the NH proton is directed to the midpoint between the O and the S atoms, the amide selects the sulfur for NH···S bonding. Figure 3 illustrates the locations of the NH protons and intraligand NH···S hydrogen bonds.

Absorption Spectra. Figure 4 shows the visible spectra of various $(NEt_4)[Mo^{V}O(SAr)_4]$ complexes in acetonitrile at room tem-

Table I. Crystallographic Data for $(PPh_4)[Mo^{V}O(S\text{-}o\text{-}CH_3CONHC_6H_4)_4]\cdot CH_3CN$ (**1a′**) and $(PPh_4)_2[Mo^{IV}O(S\text{-}o\text{-}CH_3CONHC_4H_4)_4]$ (**1b′**)

	1a′	**1b′**
chemical formula	$C_{58}H_{55}N_5O_5PS_4Mo$	$C_{80}H_{72}N_4O_5P_2S_4Mo$
fw	1157.26	1455.60
crystal system	monoclinic	monoclinic
a, Å	20.95 (2)	14.636 (3)
b, Å	12.509 (2)	13.457 (3)
c, Å	22.383 (5)	19.341 (2)
β, deg	91.8 (1)	110.08 (1)
V, Å^3	5864 (8)	3578 (1)
Z	4	2
space group	$P2_1/n$	$P2_1$
μ, cm^{-1}	4.29	3.87
temp, °C	23	23
d_{calcd}, g cm^{-3}	1.311	1.351
radian	Mo Kα	Mo Kα
$2\theta_{max}$	60.1°	60.1°
scan type	ω–2θ	ω–2θ
no. of reflcns measd		
total	18401	11290
unique	17957	10900
no. of obsd reflcns with $I > 3\sigma(I)$	6985	5201
R^a	0.052	0.048
R_w^b	0.063	0.046
GOF	2.11	1.33
no. of params	740	959

$^a R = \sum||F_o| - |F_c||/\sum|F_o|$. $^b R_w = [\sum w(|F_o| - |F_c|)^2/\sum w|F_o|^2]^{1/2}$; $w = 1/\sigma^2(|F_o|)$.

Table II. Selected Bond Distances (Å) and Angles (deg) of $(PPh_4)[Mo^{V}O(S\text{-}o\text{-}CH_3CONHC_6H_4)_4]\cdot CH_3CN$ (**1a′**) and $(PPh_4)_2[Mo^{IV}O(S\text{-}o\text{-}CH_3CONHC_6H_4)_4]$ (**1b′**)

	1a′	**1b′**
Mo=O	1.679 (4)	1.689 (5)
Mo–S(1)	2.404 (3)	2.421 (2)
Mo–S(2)	2.383 (2)	2.401 (2)
Mo–S(3)	2.407 (2)	2.408 (3)
Mo–S(4)	2.392 (3)	2.403 (2)
mean Mo–S	2.397 (10)	2.408 (8)
N(1)–S(1)	3.026 (7)	2.992 (8)
N(2)–S(2)	2.989 (5)	2.991 (8)
N(3)–S(3)	3.004 (6)	3.003 (6)
N(4)–S(4)	2.965 (5)	3.015 (8)
N(1)–O	3.182 (7)	3.22 (1)
N(2)–O	3.286 (6)	3.503 (9)
N(3)–O	3.138 (7)	3.231 (9)
N(4)–O	3.355 (7)	3.43 (1)
S(1)–Mo–S(3)	148.87 (7)	150.60 (7)
S(2)–Mo–S(4)	136.11 (6)	143.44 (7)

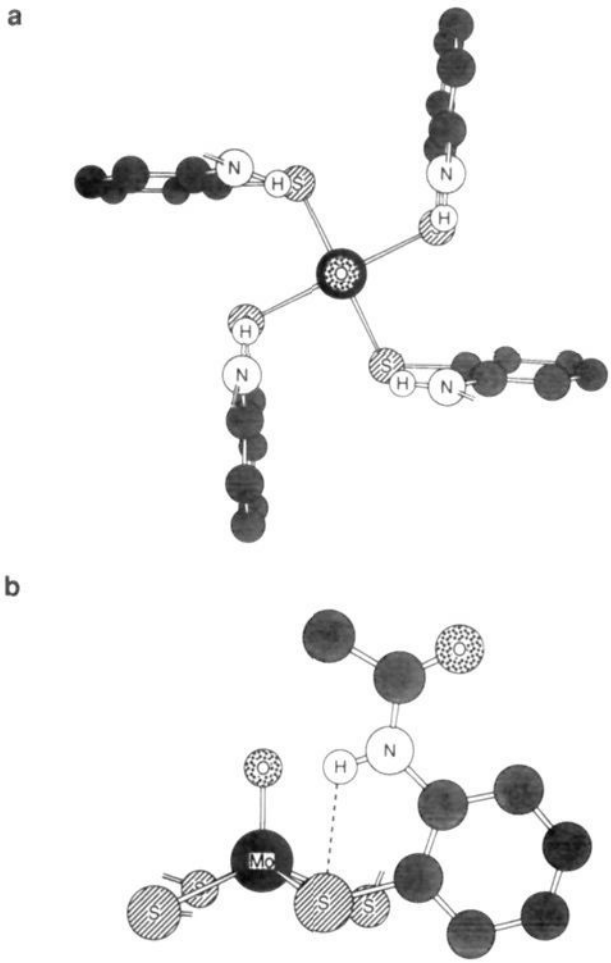

Figure 3. Intraligand NH···S interaction in $(PPh_4)[Mo^{V}O(S\text{-}o\text{-}CH_3CONHC_6H_4)_4]\cdot CH_3CN$. Acetyl groups (a) or three aryl groups (b) are omitted.

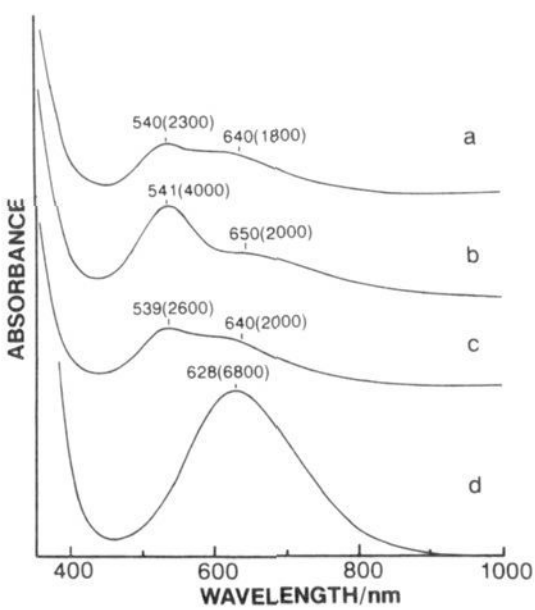

Figure 4. Visible spectra of (a) $(NEt_4)[Mo^{V}O(S\text{-}o\text{-}CH_3CONHC_6H_4)_4]$, (b) $(NEt_4)[Mo^{V}O(S\text{-}o\text{-}t\text{-}BuCONH\text{-}C_6H_4)_4]$, (c) $(NEt_4)[Mo^{V}O(S\text{-}o\text{-}CF_3CONHC_6H_4)_4]$, and (d) $(NEt_4)[Mo^{V}O(S\text{-}p\text{-}t\text{-}BuCONHC_6H_4)_4]$ in acetonitrile at room temperature.

perature. The *o*-(acylamino)benzenethiolate Mo(V) complexes shows two intense bands at 540 and 640 nm for $[Mo^{V}O(S\text{-}o\text{-}CH_3CONHC_6H_4)_4]^-$, at 541 and 650 nm for $[Mo^{V}O(S\text{-}o\text{-}t\text{-}BuCONHC_6H_4)_4]^-$, and at 539 and 640 nm for $[Mo^{V}O(S\text{-}o\text{-}CF_3CONHC_6H_4)_4]^-$ with molar coefficients (2000–6000). On the other hand, para-substituted benzenethiolate Mo(V) complex, e.g., $[Mo^{V}O(S\text{-}p\text{-}t\text{-}BuCONHC_6H_4)_4]^-$, exhibits a single peak at 628 nm similar to the absorption maximum of $[Mo^{V}O(SPh)_4]^-$ at 598 nm. Also $[Mo^{V}O(S\text{-}o\text{-}CH_3CON(CH_3)C_6H_4)_4]^-$ exhibits a single intense band at 606 nm (6200 M^{-1} cm^{-1}) as shown in Table III. The double peaks of **1a** are not due to the steric congestion by the amide group at the ortho position of arenethiolate ligand. The intensities of the double peaks of **2a** were changed depending on the temperature in the range of 0–30 °C with isosbestic points (464 and 585 nm) in acetonitrile. The intensity of absorption maximum at 541 nm was increased by cooling. The results suggest the presence of an equilibrium between isomers of which abundance depends on the temperature. The difference of the absorbances between **1a** and **2a** is considered to be caused by structural difference of $Mo^{V}OS_4$ core due to bulk *tert*-butyl groups. The ratio of two intensities of double peaks of **1a** or **2a** were slightly changed by a variation of solvent. The UV–visible spectrum of the *o*-acylamino Mo(IV) complex, **1b**, in acetonitrile (Figure 5) indicates two absorption maxima at 299 (28 000 M^{-1} cm^{-1}) and 552 nm (300 M^{-1} cm^{-1}) due to a S-to-Mo or O-to-Mo LMCT and to a d–d transition, respectively. The other Mo(IV) complexes, $(NEt_4)_2[Mo^{IV}O(S\text{-}o\text{-}t\text{-}BuCONHC_6H_4)_4]$ and $(NEt_4)_2[Mo^{IV}O(S\text{-}o\text{-}CF_3CONHC_6H_4)_4]$, show a similar spectral pattern at 300 (30 000 M^{-1} cm^{-1}) and 546 nm (250 M^{-1} cm^{-1}) and at 293 (34 000 M^{-1} cm^{-1}) and 549 nm (310 M^{-1} cm^{-1}), respectively. The d_{xy} to $d_{yz,zx}$ transition has been reported in this region for $[MoOCl_4]^-$ which shows a higher energy ligand-to-metal charge-transfer (LMCT) band.[47] Ellis et al. have established that the d–d transition in Mo(V) thiolate complex is

Table III. Absorption Maxima and Redox Potentials of Various $(NEt_4)[Mo^{V}O(SAr)_4]$ in Acetonitrile

SAr	λ_{max}, nm (ϵ, M^{-1} cm^{-1})	$E_{1/2}$, V vs SCE
S-*o*-$CH_3CONHC_6H_4$	540 (2300), 640 (1800)	−0.36
S-*o*-*t*-$BuCONHC_6H_4$	541 (4000), 650 (2000)	−0.46
S-*o*-$CF_3CONHC_6H_4$	539 (2600), 640 (2000)	−0.25
SC_6H_5	598 (6600)[a]	−0.81
S-*p*-*t*-$BuCONHC_6H_4$	628 (6800)	−0.82
S-*p*-$MeOC_6H_4$	634 (5400)	−0.88
S-*o*-$MeOC_6H_4$	619 (6200)	−0.86
S-*o*-$CH_3CON(CH_3)C_6H_4$	606 (6200)	−0.71

[a] The value was cited from ref 3.

Table IV. ESR Parameter of $(NEt_4)[Mo^{V}O(SAr)_4]$ in CH_3CN/DMF (=4:1 v/v) at 77 K

SAr	$g_{\parallel}$	$g_{\perp}$	$10^4A_{\parallel}$, cm^{-1}	$10^4A_{\perp}$, cm^{-1}
S-*o*-$CH_3CONHC_6H_4$	2.027	1.980	54.0	22.3
S-*o*-*t*-$BuCONHC_6H_4$	2.035	1.981	54.9	23.4
SC_6H_5[a]	2.017	1.979	52.3	22.3

[a] Reference 17.

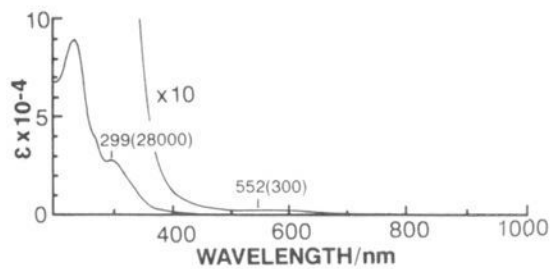

Figure 5. UV–visible spectrum of $(NEt_4)_2[Mo^{IV}O(S\text{-}o\text{-}CH_3CONHC_6H_4)_4]$ in acetonitrile at room temperature.

(47) Garner, C. D.; Hill, L. H.; Mabbs, F. E.; McFadden, D. L.; McPhail, A. T. *J. Chem. Soc., Dalton Trans.* **1977**, 853.
(48) Ueyama, N.; Zaima, H.; Nakamura, A. *Chem. Lett.* **1986**, 1099.

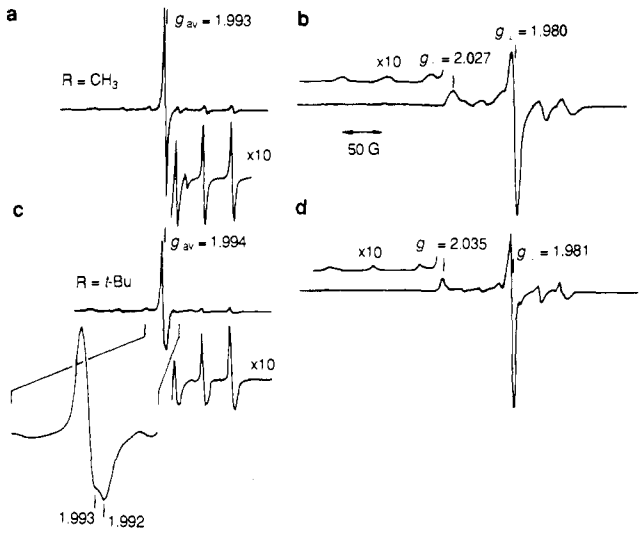

Figure 6. ESR spectra of $(NEt_4)[Mo^VO(S\text{-}o\text{-}CH_3CONHC_6H_4)_4]$ (a, b) and $(NEt_4)[Mo^VO(S\text{-}o\text{-}t\text{-}BuCONHC_6H_4)_4]$ (c, d) in acetonitrile/DMF (4/1 v/v) at 302 K (a, c) and 77 K (b, d).

Table V. Raman Bands of $(NEt_4)[Mo^VO(SAr)_4]$ and $(NEt_4)_2]Mo^{IV}O(SAr)_4]$ in Solid State

complexes	ν(Mo=O), cm^{-1}
$(NEt_4)[Mo^VO(S\text{-}o\text{-}CH_3CONHC_6H_4)_4]$	937
$(NEt_4)_2[Mo^{IV}O(S\text{-}o\text{-}CH_3CONHC_6H_4)_4]$	902
$(NEt_4)[Mo^VO(S\text{-}o\text{-}t\text{-}BuCONHC_6H_4)_4]$	947
$(NEt_4)_2[Mo^{IV}O(S\text{-}o\text{-}t\text{-}BuCONHC_6H_4)_4]$	940
$(NEt_4)[Mo^VO(S\text{-}o\text{-}CF_3CONHC_6H_4)_4]$	949
$(NEt_4)_2[Mo^{IV}O(S\text{-}o\text{-}CF_3CONHC_6H_4)_4]$	940
$(NEt_4)[Mo^VO(S\text{-}p\text{-}t\text{-}BuCONHC_6H_4)_4]$	922
$(NEt_4)[Mo^VO(S\text{-}C_6H_5)_4]$	936[a]
$(NEt_4)[Mo^VO(S\text{-}2,4,6\text{-}i\text{-}Pr_3C_6H_2)_4]$	946[a]

[a] Reference 48.

masked by the intense LMCT band due to the low energy of the LMCT band.[22] The two intense peaks at 539–540 and 640 nm in **1a** and **2a** are tentatively assigned to the Mo–S LMCT bands. Such split peaks were also observed for the LMCT bands of $[Mo^VO(\alpha,2\text{-toluenedithiolato})_2]^-$ containing two distinct Mo–S bonds, alkene– and arene–thiolato ligands.[11] The small shift of d–d transition in the Mo(IV) complexes suggests a small geometrical change of $Mo^{IV}OS_4$ core induced by steric and electronic effects of the acylamino substituent group.

ESR Spectra of $(NEt_4)[Mo^VO(SAr)_4]$ Complexes. Figure 6 shows the ESR spectra of $(NEt_4)[Mo^VO(S\text{-}o\text{-}CH_3CONHC_6H_4)_4]$ (**1a**) and $(NEt_4)[Mo^VO(S\text{-}o\text{-}t\text{-}BuCONHC_6H_4)_4]$ (**2a**) in acetonitrile/DMF (4/1) at 302 and 77 K. The ESR parameters are listed in Table IV and compared with those of $(NEt_4)[Mo^VO(SPh)_4]$ at 77 K.[17] Ortho-substituted thiolate Mo(V) complexes (**1a** and **2a**) have a tendency to exhibit large $g_{\parallel}$ values (2.027 and 2.035, respectively). **1a** and **2a** exhibited axial signals even in a C_2 local structure as determined by the crystallographic analysis, which is different from the tetragonal-pyramidal. Garner et al. have demonstrated that the g tensors coincide to the Mo–O directions in the various Mo(V) complexes.[47] The large $g_{\parallel}$ values should reflect the ligand field equatorial to the Mo–O bond axis because of spin-orbit coupling between Mo and sulfur. The distorted Mo^VOS_4 core with narrow S–Mo–S angle in **1a** is ascribed to a large $Mo(d_{xy})$–S(p) π-interaction with mixing of p_z and d_{z^2} orbitals with contribute to the increasing $g_{\parallel}$ value. $(NEt_4)[Mo^VO(\alpha,2\text{-toluenedithiolato})_2]$ having the same type of distorted Mo^VOS_4 local structure also exhibited a large $g_{\parallel}$ value (2.035).[11]

The spectrum (Figure 6) of **2a** at 302 K indicates the presence of another isomer at g_{av} = 1.993 although no signal for the isomer was observed at 77 K. In the case of **1a**, no new signal was observed even at 302 K. The results indicate that another conformational isomer of **2a**, different from the X-ray crystallographically determined structure of **1a**, occurs at higher temperature in solution.

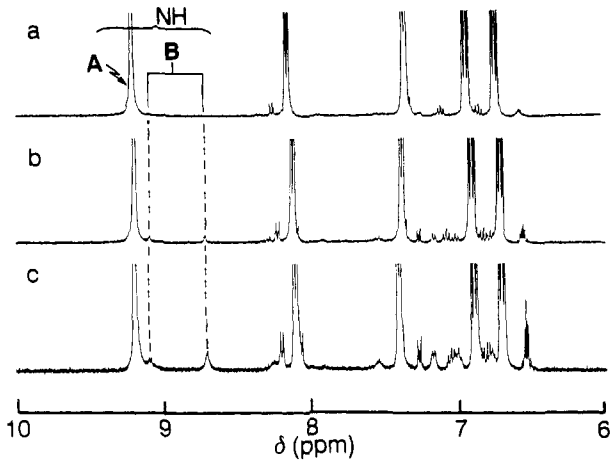

Figure 7. Temperature dependence of ^1H NMR spectra of $(NEt_4)_2[Mo^{IV}O(S\text{-}o\text{-}t\text{-}BuCONHC_6H_4)_4]$ in acetonitrile-d_3 at (a) 233, (b) 273, and (c) 303 K. A and B indicate NH proton signals for conformational isomers A and B shown in Figure 9, respectively.

IR and Raman Spectra. Table V lists the Mo=O stretching bands of **1a**, **2a**, and the related compounds in solid state. A significant difference (10 cm^{-1}) between **1a** and **2a** was observed in the Raman spectra. The higher wavenumber shift has been ascribed to the less π-donor ability of substituted arenethiolate ligand for $[Mo^VO(SR)_4]^-$ (SR = SPh, S-4-$CH_3C_6H_4$, S-4-ClC_6H_4, S-3-ClC_6H_4, S-4-FC_6H_4, S-2,6-$Cl_2C_6H_3$, and SC_6F_5).[22] A higher Mo=O stretching value has been reported for $[Mo^VO(tipbt)_4]^-$ (tipbt = 2,4,6-triisopropylbenzenethiolato, S-2,4,6-i-$Pr_3C_6H_2$) which contains bulky groups at the ortho position. The higher shift has been considered to be caused by the less electron-donating thiolato coordination through hindered conjugation,[48] which may also be invoked to interpret the difference between **1a** and **2a**.

A lower Mo=O stretching value for $[Mo^{IV}O(SC_6F_5)_4]^{2-}$ compared to the corresponding Mo(V) complex has been reported. The weakness of the Mo=O bonding has been considered to be due to decrease in O($p\pi$) to Mo($d\pi$) donation.[22] Since no significant or small change of Mo=O distance is observed in our complexes for in the two redox states, Mo(V) and Mo(IV), the large difference (35 cm^{-1}) in ν(Mo=O) comes from other reason which is probably associated with the distorted Mo^VOS_4 local structure. The IR bands for the NH stretching of **1a** and **1b** were observed at 3335 and 3330 cm^{-1}, respectively. The disulfide, 2,2′-dithiobis(*N*-phenyl-2,2-dimethylpropanamide), exhibits the NH bands at 3389 and 3251 cm^{-1} assignable to free and intermolecular NH···O=C hydrogen bonding NH groups, respectively. The high wavenumber shift of the stretching for the complexes from that of the free NH group suggests the presence of the NH···S hydrogen bond.

Temperature Dependence of ^1H NMR Spectra of $(NEt_4)_2[Mo^{IV}O(S\text{-}o\text{-}t\text{-}BuCONHC_6H_4)_4]$ (2b). Well-defined sharp ^1H NMR peaks were obtained for $(NEt_4)_2[Mo^{IV}O(S\text{-}o\text{-}CH_3CONHC_6H_4)_4]$ (**1b**) and **2b** in acetonitrile-d_3 because of their low-spin d^2 configuration. Figure 7 shows the temperature dependence of ^1H NMR spectra of **2b**. The amide NH signal is observed at 9.21 ppm at 233 K. Two new NH signals appear at 9.09 and 8.72 ppm with the increase in temperature. The results are related to the ESR data of **2a** at 302 and 77 K. The isomer appears to result from the steric barrier to rotation about the S–C bond because the high field NH signals at 8.72 ppm indicates absence of the specific shielding from Mo=O bond. The NH signals for the isomers did not coalesce with the main NH signal even above 323 K.

Redox Potential of Mo(V)/Mo(IV). Figure 8 shows the cyclic voltammograms of a series of $(NEt_4)[Mo^VO(SAr)_4]$ complexes in acetonitrile at room temperature. Table III lists the redox potentials of the above complexes and the related complexes, e.g., $(NEt_4)[Mo^VO(S\text{-}o\text{-}CF_3CONHC_6H_4)_4]$. The Mo(IV) complexes,

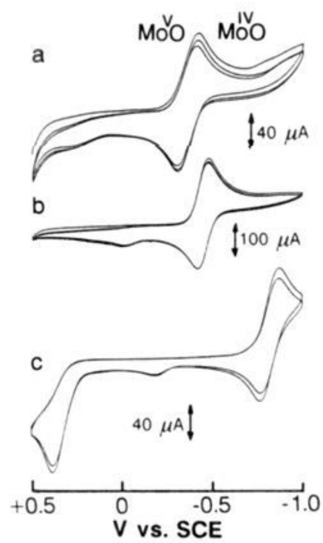

Figure 8. Cyclic voltammograms of various $(NEt_4)[Mo^{V}O$(S-*o*- or *p*-substituted (acylamino)$C_6H_4)_4]$ in acetonitrile at room temperature. The ligands are (a) S-*o*-$CH_3CONHC_6H_4$, (b) S-*o*-*t*-$BuCONHC_6H_4$, and (c) S-*p*-*t*-$BuCONHC_6H_4$, respectively. Conditions: [Mo] = 2.5 mM, $[(n\text{-}Bu)_4NClO_4]$ = 0.1 M, scanning rate, 100 mV/s.

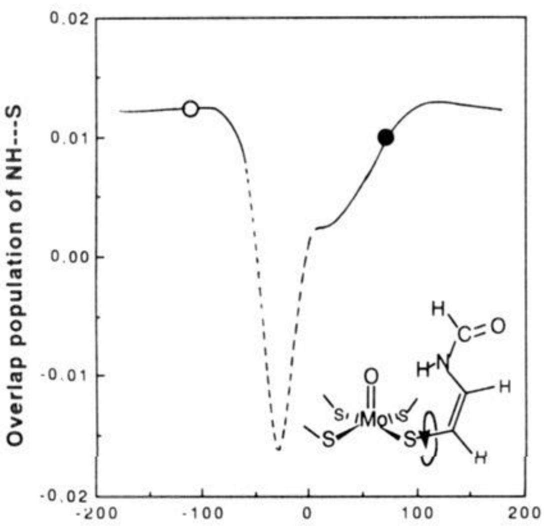

Figure 9. Variation of NH···S overlap population with change of S–C torsion angle in $[Mo^{V}O(S\text{-}o\text{-}CH_3CONHC_6H_4)_4]^-$. $[Mo^{V}O(cis\text{-}SCH{=}CHNHCHO)_4]^-$ was employed as a model complex. The broken line indicates an improbable region due to the intramolecular contact between the substituent groups. The value (●) at 72.8° and that (○) at −107.2° are shown, which are described in the text.

e.g., **1b**, show the same redox potential as that of the corresponding Mo(V) complexes. No significant difference between (NEt_4)-$[Mo^{V}O(S\text{-}o\text{-}OMeC_6H_4)_4]$ (−0.86 V vs SCE and $(NEt_4)[Mo^{V}(S\text{-}p\text{-}OMe\text{-}C_6H_4)_4]$ (−0.88 V vs SCE) was observed. The $(NEt_4)[Mo^{V}O(SAr)_4]$ complexes having an amide NH group at the ortho position of a benzenethiolate ligand exhibit the extremely positively shifted redox potentials. An amide NH at the para position barely gives a significant positive shift of the redox potential. The redox potential of −0.71 V vs SCE for $[Mo^{V}O\{S\text{-}o\text{-}CH_3CON(CH_3)C_6H_4\}_4]^-$ indicates that the amide NH is crucial for the positive shift of redox potential.

EHMO Calculations of $[Mo^{V}O(cis\text{-}SCH{=}CHNHCHO)_4]^-$. EHMO calculations were carried out to confirm the bond formation between amide NH and the sulfur atom and a preferable route, through the benzene ring or the NH···S hydrogen bond, for the amide groups to interact with the sulfur orbitals. The reported crystal structure of $[Mo^{V}O(SPh)_4]^-$ indicates the location

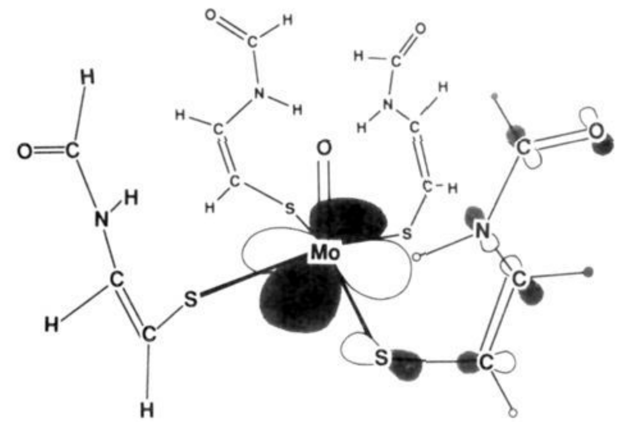

Figure 10. Schematic drawing of the SOMO for $[Mo^{V}O(cis\text{-}SCH{=}CHNHCHO)_4]^-$ of which Mo–S–C–C torsion angle is 72.8°. Lobes for only one thiolato ligand are shown. Ones for the other thiolato ligands are omitted.

of each phenyl plane facing toward the middle between the O and S atoms. Accordingly, the variation of NH···S overlap population with a change in the S–C torsion angle was estimated. The results are shown in Figure 9. Because the S–C and O–Mo bonds are not in the same plane, the unsymmetrical curve in Figure 9 is necessary. The range of about −60 to 30° is an improbable region due to the intramolecular contact between the substituent groups. The Mo–S–C–C torsion angle (72.8°) determined by X-ray analysis of **1a′** is within the angles (−180 – −60°, 30–180°) suitable for the NH···S bond formation. The calculation results indicate that the overlap population (0.010) at the Mo–S–C–C torsion angle (72.8°) is similar to that (0.012) in the opposite location (−107.2°) on the rotation about the S–C bond. A schematic drawing of the model complex at the torsion angle of 72.8° with the SOMO (singly occupied molecular orbital) shown in Figure 10 illustrates the situation. It should be noted that EHMO calculation is less quantitative in predicting energy levels and electron populations. Therefore the other appropriate methods of calculations are necessary to estimate correct electron populations at the ligand or near the NH···S hydrogen bond. This preliminary calculations, however, should be viewed as qualitative results. In addition, a simplified system such as $[MoO(SH)_4]^-$ also gave similar results for molecular orbitals of $MoOS_4$ core.

Discussion

Structural Change between $[Mo^{V}O(S\text{-}o\text{-}CH_3CONHC_6H_4)_4]^-$ and $[Mo^{IV}O(S\text{-}o\text{-}CH_3CONHC_6H_4)_4]^{2-}$. The small difference between Mo=O distances of the Mo(V) and Mo(IV) states is reasonable because the nonbonding orbital (d_{xy}) is occupied by one (in Mo(V)) or two (in Mo(IV)) electrons. If one electron enters into the next higher energy levels, d_{xz} and d_{yz}, the Mo=O character should vary because of the occupancy at these antibonding orbitals. Similarly, almost the same Mo=O distances in $(NEt_4)[Mo^{V}O$-$(SPh)_4]$ and **1a** is explicable by lack of participation of the electron-donating amide group to Mo=O bonding orbitals.

In view of this point, the remarkable difference between the Mo=O distances of $[Mo^{V}O(bdt)_2]^-$ and $[Mo^{IV}O(bdt)_2]^{2-}$ in the solid state is probably due to the slight variations of the two structure. Actually, the geometries of two bdt planes in $[Mo^{V}O(bdt)_2]^-$ have been reported to not be identical and unsymmetrical relative to the Mo=O axis. Further study will be necessary for an explanation.

A distortion of the $Mo^{V}OS_4$ core has been found in $[Mo^{V}O$-$(SCH_2CH_2CH_2S)_2]^-$ and $[Mo^{V}O(\alpha,2\text{-toluenedithiolato})_2]^-$, which has been considered to be due to the chelating effect of the unsymmetrical dithiolate ligand for the latter complex. Interestingly, although **1a** has four equivalent aromatic thiolate ligands, two Mo–S bonds are short and two Mo–S bonds are long as observed in the above two complexes. The two short Mo–S bonds trans to each other have a small S–Mo–S angle (136.1 (1)°), whereas the two long trans Mo–S bonds form a large S–Mo–S angle (148.9

Chart I

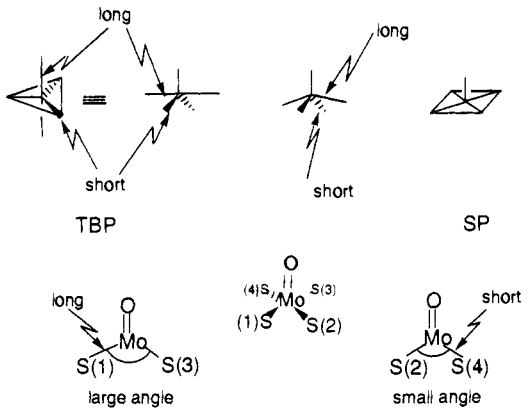

(1)°). The same trend was found in the crystal structure of $[Mo^{V}O(\alpha,2\text{-toluenedithiolato})_2]^-$. The observed distortion results in an intermediate structure between trigonal-bipyramidal and square-pyramidal as shown in Chart I.

The distortion of $Mo^{V}OS_4$ core described above is thus ascribed to partial transformation of the geometry from square-pyramidal to trigonal-bipyramidal accompanied with NH···S hydrogen bonding but not to the steric congestion of the bulky amide groups as the ortho position of arenethiolate ligand.

Stabilization of Mo–S Bond by NH···S Hydrogen Bond. The influence of NH···S hydrogen bonding on the Mo–S bond is illustrated in Figure 10 which shows the SOMO for a model complex, $[Mo^{V}O(cis\text{-}SCH{=}CHNHCHO)_4]^-$. Here, the singly-occupied d_{xy} orbital of Mo atom and the filled p_π orbital of S atom interact each other in an antibonding manner. On the other hand, the orientation of orbitals for S···H–N–C arrangement indicates stabilization for an NH···S hydrogen bond. Because of the antibonding character, any $d_\pi(Mo)$–$p_\pi(S)$ interaction destabilizes the SOMO as described in the literature.[12] Since the NH···S hydrogen bond stabilizes the sulfur p_π donor orbital to diminish the antibonding character of Mo–S bond, it strengthens the Mo–S bond consequently.

The observed shorter Mo^{V}–S(2) and Mo–S(4) bond (mean 2.388 Å) compared to Mo–S bonds (mean 2.403 Å) in $[Mo^{V}O(SPh)_4]^-$[4] nicely supports this situation, although the mean value (2.397 Å) of the four Mo–S distances for **1a** is not largely different from that for $[Mo^{V}O(SPh)_4]^-$. The small difference is considered to be ascribed to the geometrical difference between the two complexes: **1a** contains two relatively small O–Mo–S angles (105.7, 105.4°) and two large ones (111.6, 112.3°). On the other hand, $[Mo^{V}O(SPh)_4]^-$ has almost same O–Mo–S angles (108.5, 109.5, 110.2, 111.2°) which are near to the large angles in **1a**.[4] The two small O–Mo–S angles provide longer Mo–S bonds (2.404, 2.407 Å) compared to the others (2.383, 2.392 Å). Such small O–Mo–S angles (mean 105°) were reported for $[Mo^{V}O(\alpha,2\text{-toluenedithiolato})_2]^-$ which shows the similar distorted geometry of **1a**.[11] From these results, a small O–Mo–S angle is considered to give a long Mo–S bond. In the case of **1a**, the two small O–Mo–S angles make the corresponding two Mo–S bonds long and result in a little short mean Mo–S bond length in spite of the stabilization of NH···S hydrogen bonds.

In the case of Mo(IV) complex, the antibonding $d_\pi(Mo)$–$p_\pi(S)$ orbital is filled with two electrons weakening the Mo–S bond. Actually, longer mean Mo–S bonds in the Mo(IV) complex by ca. 0.01 Å compared to that in Mo(V) one were observed.

Positive Shift of Redox Potential by NH···S Hydrogen Bonding. The crsytal structures of **1a′** and **1b′** show that the amide NH points to the sulfur $p\pi$ orbital that is perpendicular to the C–S–Mo plane and that a NH···S hydrogen bond forms with 2.98–3.02 Å distances in both oxidation states. Preliminary EHMO calculations indicate the bonding character between the sulfur and NH atoms. An intermolecular NH···S hydrogen bond of this type has been reported in $[(CH_3)_3NCH_2CONH_2]_2[Co(SC_6H_5)_4]\cdot{}^1/_2CH_3CN$[37] and an intramolecular one in $[\mu\text{-}N_2H_4\{Fe(bdt)_2\}_2]^{2-}$.[38]

The presence of an amide NH group at the ortho position of an arenethiolate ligand contributes to the remarkable positive shift of redox potential of Mo(V)/Mo(IV) couple. The positive shift is not due to the steric congestion which follows the $Mo^{V}OS_4$ core distortion and the change of the SOMO energy. Substitution of the NH group with NCH_3 dramatically restores the redox potential to a more negative value, e.g., from −0.36 V (vs SCE) in **1a** to −0.71 V in $[Mo^{V}O\{S\text{-}o\text{-}CH_3CON(CH_3)C_6H_4\}_4]^-$.

The electronic substituent effect of an arenethiolate on the redox potential has been established for $[Mo^{V}O(SR)_4]^-$ (SR = SPh, S-4-$CH_3C_6H_4$, S-4-ClC_6H_5, S-3-ClC_6H_4, S-4-FC_6H_4, S-2,6-$Cl_2C_6H_3$, and S-C_6F_5) by Garner et al.[22] They found a positive shift of redox potential by the electron-withdrawing group. In our case, the large difference in the redox potential between −0.36 V (vs SCE) for **1a** and −0.82 V for $[Mo^{V}O(S\text{-}p\text{-}t\text{-}BuCONH\text{-}C_6H_4)_4]^-$ indicates the significance of the NH···S hydrogen bonding rather than a simple electronic effect.

The presence of NH···S hydrogen bonds have been reported in the crystallographic analyses of *Peptococcus aerogenes* ferrodoxin, *Chromatium vinosum* high potential iron potential, and *Spirulina platensis* plant-type ferredoxin. The role of the NH···S hydogen bonds has been demonstrated by $[Fe_4S_4(Z\text{-cys-Gly-Ala-OMe})_4]^{2-}$ as a model of ferredoxin and by $[Fe^{II}(Z\text{-cys-Pro-Leu-cys-Gly-NH-}p\text{-substituted anilide})_2]^{2-}$ as a model of reduced rubredoxin. It is probable that the redox potential of a biologically relevant monooxomolybdenum(V) thiolate complex is also controlled by the NH···S hydrogen bonding.

Direct participation of the NH···S hydrogen bond in the positive shift is supported by the more positively shifted redox potential (−0.25 V vs SCE) of $[Mo^{V}O(S\text{-}o\text{-}CF_3CONHC_6H_4)_4]^-$, which indicates that the strong electron-withdrawing power of CF_3 strengthens the hydrogen bond through the amide group. The EHMO calculations also support the participation of the hydrogen bond in stabilizing the p_π orbitals on S through the S···H–N–C–O–CF_3 route (Figure 10).

The Location of Acylamino Groups. The interaction between Mo=O and amide NH groups as described above is considered an unlikely possibility. The results of EHMO calculations indicate that the lack of an oxygen atomic orbital in the SOMO. The negative NH···O=Mo overlap population (−0.0003) shows a weak repulsion between them. In addition, Mo=O bond has been reported to have a triple bond character with ligand-to-metal charge-transfer $Mo(d_{xy,yz})$–$O(p_{x,y})$,[1] which is formally expressed as $Mo{\equiv}O^+$. Such a slightly positively charged oxygen atom is unlikely to interact with a positively polarized amide proton. Therefore, the direct attractive interaction between the oxo ligand and NH is considered to be absent.

One possible explanation is proposed here for the location of the acylamino group. An amide group has a dipole moment, $-NH^{\delta+}$–$CO^{\delta-}$–, and the Mo=O group is considered to have a small dipole moment, $Mo^{\delta-}{\equiv}O^{\delta+}$, due to the triple bond character. These dipoles are likely to interact with each other to minimize the total intramolecular dipole moment. The stabilizing interaction is maximized in an antiparallel orientation and minimized in a parallel one. The location of the acylamino group at the Mo=O side maximizes the sum of the stabilizing electrostatic interactions and the opposite location minimizes it. The stabilization by this interaction competes with destabilization by the steric congestion between acylamino groups. Actually, a bulkyl acylamino group, *t*-BuCONH–, cannot sufficiently stabilize the location faced to Mo=O group as described below.

Isomerization by Bulky Amide. The crystal analysis of **1a′** indicates that all the ortho substituted amide groups are located at the same side as the Mo=O group in the solid state. However, $[Mo^{V}O(S\text{-}o\text{-}t\text{-}BuCONHC_6H_4)_4]^-$ has another isomer in solution at room temperature as detected by ESR spectroscopic analysis. The shift of the g_{av} value is ascribed to the low symmetry by the isomerization which probably exhibits anisotropic signal through the deviation of the direction of the *g* tensor from the Mo=O axis. In the symmetrical isomer, the *g* tensor exists along the Mo=O axis.

The isomerization of $[Mo^{IV}O(S\text{-}o\text{-}t\text{-}BuCONHC_6H_4)_4]^{2-}$ occurs in acetonitrile as illustrated in Figure 11. At higher temperature

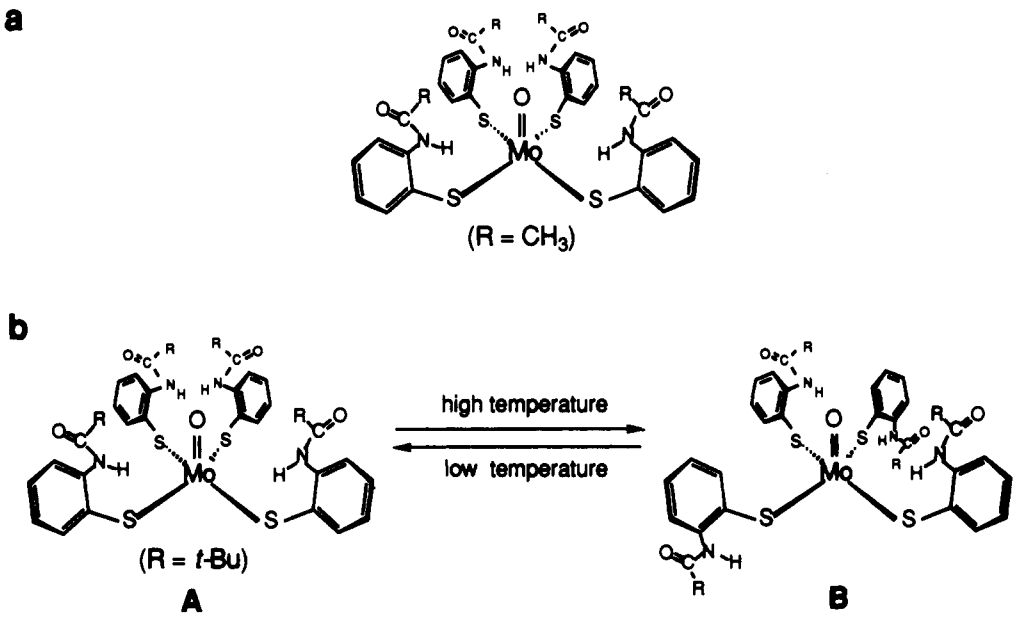

Figure 11. Schematic drawing for (a) $[Mo^{IV}O(S\text{-}o\text{-}CH_3CONHC_6H_4)_4]^{2-}$ without conformational change and (b) $[MoO^{IV}(S\text{-}o\text{-}t\text{-}BuCONHC_6H_4)_4]^{2-}$ on variable conformational change.

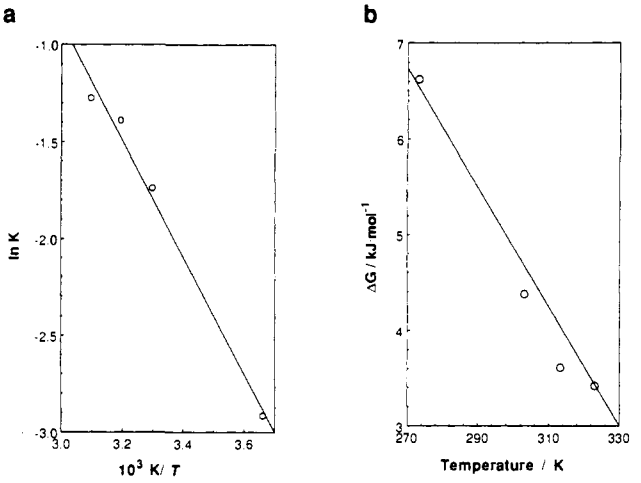

Figure 12. Plot of kinetic parameters against temperature in the conformational change of $(NEt_4)_2[Mo^{IV}O(S\text{-}o\text{-}t\text{-}BuCONHC_6H_4)_4]$. Two fitting lines are (a) $\ln K = 8.17\text{–}3.20 \times 10^3/T$ and (b) $\Delta G = 24.9\text{–}0.067T$, respectively.

the isomer B is formed across the barrier. The thermodynamic parameters for this equilibrium were estimated from the change of NH signal intensity. Figure 12 plots the data, and calculated values of ΔH and ΔS are 25 ± 2 kJ mol^{-1} and 67 ± 7 J K^{-1} mol^{-1}, respectively. The positive large ΔS indicates this isomerization is an entropy-controlled reaction. The activation energy, ΔE, could not be calculated because of the lack of coalescence of the signals even above 323 K.

Conclusion

The presence of NH···S hydrogen bonds $[Mo^{V}O(S\text{-}o\text{-}CH_3CONHC_6H_4)_4]^-$ and $[Mo^{IV}O(S\text{-}o\text{-}CH_3CONHC_6H_4)_4]^{2-}$ was established by X-ray crystallographic and IR analyses. The NH···S hydrogen bond contributes to the positive shift of redox potential for Mo(IV)/Mo(V) even in a high dielectric solvent, e.g., DMF. The positive shift provides a practical advantage for the synthesis of the Mo(IV) complex from the corresponding Mo(V) complex with weak reductants. The positive shift with the NH···S hydrogen bond is essential for the control of the redox potential of biologically important metalloproteins and metalloenzymes even if their structures are different from these complexes. Actually, the hair-pin turn chelation of peptide ligands, e.g., Cys-X-Y-Cys (X, Y = amino acid residues) in rubredoxin, forces the amide NH group to point to the sulfur atom just as the *o*-(acetylamino)benzenethiolate ligand does.

Supplementary Material Available: Listings of final positional and thermal parameters and intramolecular bond angles and distances for **1a′** and **1b′** (37 pages); listings of final observed and calculated structure factors (84 pages). Ordering information is given on any current masthead page.